ACS OMEGA

Article

Cite This: ACS Omega 2019, 4, 4147−4152

http://pubs.acs.org/journal/acsodf

# Thermal Transport Engineering in Graphdiyne and Graphdiyne Nanoribbons

Yingchun Wan,[†,∥] Shiyun Xiong,[†,∥] Bin Ouyang,[‡] Zhihui Niu,[†] Yuxiang Ni,[§] Yu Zhao,*[,†] and Xiaohong Zhang*[,†]

[†]Institute of Functional Nano & Soft Materials (FUNSOM), Jiangsu Key Laboratory for Carbon-Based Functional Materials & Devices, Soochow University, 199 Ren'ai Road, Suzhou, 215123 Jiangsu, P. R. China

[‡]Department of Materials Science and Engineering, University of California Berkeley, Berkeley, California 94720, United States

[§]School of Physical Science and Technology, Key Laboratory of Advanced Technologies of Materials, Ministry of Education of China, Southwest Jiaotong University, 610031 Chengdu, P.R. China

**ABSTRACT:** Understanding the details of thermal transport in graphdiyne and its nanostructures would help to broaden their applications. On the basis of the molecular dynamics simulations and spectrally decomposed heat current analysis, we show that the high-frequency phonons in graphdiyne can be strongly hindered in nanoribbons because of the boundary scattering. The isotropic transport in graphdiyne can be switched to anisotropic along the armchair and zigzag directions. Adding side chains onto the nanoribbon edges further reduces the thermal conductivity (TC) along both armchair and zigzag directions thanks to the reduction of heat current carried by low-frequency modes, a mechanism that arises from the phonon resonances. The uniaxial tensile strain plays a different role in the TC of graphdiyne, armchair nanoribbons, and zigzag nanoribbons. Tensile strain causes the thermal conductivities of graphdiyne, and armchair nanoribbons increase first and then get reduced, whereas for zigzag nanoribbons, the TC decreases with strain first and reaches to a plateau. The different low-frequency phonon response on strain is the main reason for the different TC behavior. For graphdiyne and armchair nanoribbons, the low-frequency heat current is enhanced gradually first and then get reduced with the increase of strain, while that of zigzag nanoribbons decreases with strain and then increases slightly. The current studies could help us understand the phonon transport in graphdiyne and its nanoribbons, which is useful for their TC engineering.

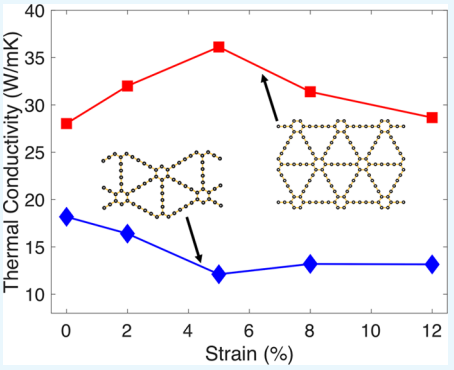


## 1. INTRODUCTION

Graphynes (GYs), which are two-dimensional (2D) structures assembled by sp- and $sp^2$-hybridized carbon atoms, have attracted great attention because of their distinguished mechanical, optical, thermal, and electronic properties.[1] GYs have been applied in many fields such as rechargeable batteries,[2,3] solar cells,[4] thermoelectric materials,[5−7] and so forth. In these applications, the thermal transport property of GYs is an important factor for the stability and/or performance of the corresponding devices. For example, overheating is a common phenomenon in rechargeable batteries and it can affect the battery stability or even lead to explosions during the service. As a result, GYs should have high thermal conductivity (TC) to avoid thermal accumulation for battery application. On the other hand, GYs should behave as "phonon glass" to maximize the performance in thermoelectric applications. The study of thermal transport property of GYs has been performed by several researchers. Using the Green's function calculations, Ouyang et al. have demonstrated that the thermal conductance of armchair $\beta$-GY nanoribbons presents abnormal stepwise width dependence.[5] On the basis of first-principles calculations and molecular dynamics simulations, Shi et al.[6,7] have investigated the thermal transport of $\gamma$-GY and graphdiyne (GDY) at room temperature. They have found that the TC of $\gamma$-GY and GDY is much different, demonstrating the tunability of TC by the number of ethynyl units. The effect of acetylenic linkages on the TC of GYs has also been confirmed by Zhang et al.[8] They have found that the presence of acetylenic linkages in GYs leads to a significant reduction of TC as a result of the associated low atom density in the structures and weak single bonds in the acetylenic linkages. Although the overall TC of different GY structures has been reported, the detailed information on thermal transport, especially the heat carried by the modes of different frequencies, is yet to be investigated. Such information is quite necessary for better understanding and engineering the thermal transport of GYs. Besides, strain is inevitable in devices because of its atomic thin nature. Actually, strain engineering has become a useful and important strategy to improve the materials performance.[9−15] As a result, it is also important to study the effect of strain on the thermal transport of GYs and related structures. Moreover, our previous work shows that by forming side branches on nanostructures, it is

Received: January 9, 2019
Accepted: February 14, 2019
Published: February 25, 2019






DOI: 10.1021/acsomega.9b00074
ACS Omega 2019, 4, 4147−4152

possible to design resonant modes which can hinder the propagation of low-frequency phonons.[16,17] Actually, side branches in 2D materials have been shown to be robust in thermal transport engineering.[18−20] Differing from the branches added to the main structure in previous studies, GYs possess single-atom branches composed of single and triple bonds when downsizing it to nanoribbons in a proper way. Because those side branches are in atomic size, which is much thinner than the traditionally considered resonant structures, their ability on producing the resonant modes is yet to be clarified.

In this work, taking GDY as an example, we perform a comprehensive study on the thermal transport of GDY and GDY nanoribbons using nonequilibrium molecular dynamics (NEMD) simulations. The spectrally decomposed heat current (SDHC) is analyzed for the cases with and without lattice strain. We show that although the TC of GDY is isotropic, the TCs of its nanoribbons along the armchair and zigzag directions are much different. The SDHC demonstrates that the difference arises from the phonons at low frequencies, indicating that a different strategy should be used for TC engineering along the two directions.

## 2. RESULTS AND DISCUSSION

To calculate the TC with NEMD, different sample lengths along zigzag and armchair directions are constructed. Figure 1a,c is the schematic of the constructed nanoribbons along the armchair and zigzag directions. The widths of the nanoribbons along the armchair and zigzag directions are chosen as 8.9 and 9.8 nm, respectively. To study the edge effect on thermal transport, we add side chains that involve a single and triple bond on the edges of armchair and zigzag nanoribbons, which correspond to Figure 1b,d, respectively. It is worth to note that we did not passivate the dangling bonds on the nanoribbon edges with hydrogen atoms. The passivation of H atoms will reduce the TC of all structures; however, it will not affect the trends of our results. Moreover, H atoms are much lighter than carbon atoms; thus, a much smaller time step is required if H atoms are included, leading to a much heavier simulation. As a result, we do not consider the passivation of nanoribbon edges. All simulations are conducted with the LAMMPS code.[21] The adaptive intermolecular reactive empirical bond order (Airebo) potential[22] is adopted to describe the interatomic interactions and a time step of 0.5 fs is adopted. The atoms at the two ends of the samples are fixed to eliminate the drift of systems. Next to the fixed layers, the atoms within the length $L_{bath}$ in the left side and right side are, respectively, coupled to hot and cold Langevin heat baths. The coupling constant is set to $\tau_{bath}$ = 1 ps and the minimum bath length $L_{bath}$ is 32 nm. All TCs are calculated at the mean temperature $T$ = 300 K. The simulation time for the systems to reach to the nonequilibrium steady state ranges from 10 to 50 ns, depending on the length of the systems. The energy $E$ injected into the hot bath and subtracted from the cold bath is recorded for 10 ns of simulations after the system reached steady state, the heat flux $J$ is extracted as $J = dE/dt/S$, where $S$ is the cross section of the samples, and a thickness of 3.5 Å is used for all cases. With the heat flux and temperature gradient, the TC can be evaluated based on Fourier's law

$$\kappa = -\frac{J}{\partial T/\partial z} \tag{1}$$

Because of the ballistic transport feature of the phonons with a mean-free path larger than the system length, the TC obtained from NEMD simulations is size-dependent. To obtain the intrinsic TC corresponding to the situation of infinite long samples, one needs to extrapolate the TCs of the samples with finite sizes to infinite length. On the basis of Matthiessen's rule, Sellan et al.[23] have derived an extrapolation strategy

$$\frac{1}{\kappa(L)} = \frac{1}{\kappa(\infty)} + \frac{\alpha}{L} + \frac{\beta}{L^2} + \dots \tag{2}$$

where $\kappa(L)$ and $\kappa(\infty)$ correspond to the TCs of the samples with length $L$ and infinite, respectively. $\alpha$ and $\beta$ are the fitting parameters. Usually, only the first two parts are kept in eq 2; thus, a linear relationship between $1/\kappa(L)$ and $1/L$ is obtained,

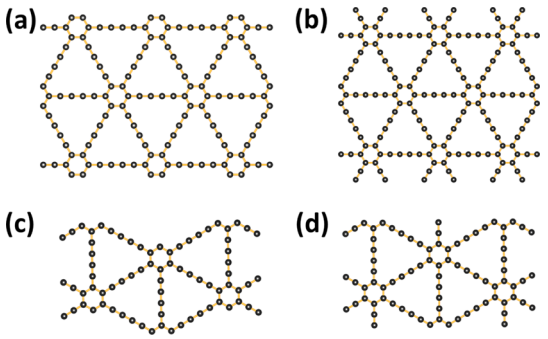


**Figure 1.** Schematic representation of the simulated nanoribbon structures. Structures (a,c) are nanoribbons along the armchair and zigzag directions, respectively. Structures (b,d) are constructed based on structures (a,c), respectively, by adding side chains onto the edges.

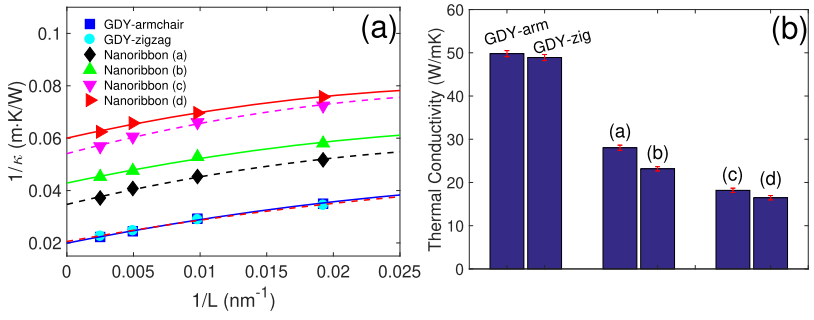


**Figure 2.** (a) Extrapolation of $1/\kappa$ vs $1/L$ with eq 2 for GDY and GDY nanoribbons; (b) Extrapolated TCs of GDY along armchair and zigzag directions as well as the nanoribbons illustrated in Figure 1.



DOI: 10.1021/acsomega.9b00074
ACS Omega 2019, 4, 4147−4152

which works very well in most cases. However, when the mean-free path of phonons distributes in a broad range and the simulated lengths are much shorter than the long mean-free path, the linear relation cannot fit the length-dependent TC with high accuracy. In our simulations, we obtained the TCs for samples with lengths ranging from 22 to 400 nm (the results for 22 nm are not shown in Figure 2a). Indeed, we found that in this length range, the dependence of $1/\kappa(L)$ on $1/L$ cannot be well described by the linear relationships. The $R^2$ factor, which describes the goodness of fitting, is smaller than 0.94 ($R^2$ approaches to 1 for a good fitting). Instead, a quadratic fitting described by eq 2 (with higher orders of $1/L$ neglected) could fit our length-dependent TC much better as shown in Figure 2a. For all quadratic fittings, the $R^2$ is larger than 0.998, indicating a very accurate fitting.

The nonlinear behavior of $1/\kappa$ versus $1/L$ is more pronounced for short sample lengths. As a result, using the linear extrapolation strategy for short samples usually will underestimate the TC.[24] For long samples, the deviation from the linear relationship of $1/\kappa$ from $1/L$ is small. Actually, Dong et al.[24] demonstrated that if the sample length is larger than the phonon mean-free path, one can get an accurate extrapolation with the linear fitting strategy. However, one needs to simulate the TC for several long samples, which is computationally expensive, especially for high TC materials. Alternatively, we suggest to use the quadratic extrapolation strategy based on the TCs of samples with lengths around the phonon mean-free path, which might be useful to compromise between the problems of heavy simulations and the accuracy when a nonlinear behavior is found.

Figure 2b demonstrates the extrapolated TCs for each case. For 2D GDY, the thermal transport is isotropic along the armchair and zigzag directions with the value of 50 W/m K. However, when downsizing into nanoribbons, the TC becomes anisotropic and is greatly reduced because of the strong phonon boundary scattering. For nanoribbons along the armchair (Figure 1a) and zigzag (Figure 1c) directions, the TCs are only 28.0 and 18.2 W/m K, respectively. The large anisotropic transport arises from the different boundary environment, that is, the nanoribbons along the armchair direction possess much flat edges compared to those along the zigzag direction; thus, the scattering of phonons by the armchair edges weakens. In our previous work, we found that the surface structures of nanowires[16] and thin films[17] could affect the thermal transport noticeably because of the resonant hybridization effect. To study the effect of edge structures on the thermal transport of the GDY nanoribbons, we added side chains composed of a single and triple bond on the edges of nanoribbons (a,c). The resulting structures are illustrated by Figure 1b,d, and the corresponding TCs are demonstrated in Figure 2b. With the additional chains, the TCs of GDY nanoribbons along both armchair and zigzag directions are reduced, revealing that adding materials properly could hinder the thermal transport of GDY nanoribbons. The observed phenomenon offers a further possibility for the engineering of nanoribbon TC.

To understand how the edges affect the phonon transport at different frequencies, we calculated the frequency-resolved heat current of GDY along the armchair direction and GDY nanoribbons based on the NEMD simulations. The heat flux $q_{L\to R}(\omega)$ across the interface of two adjacent blocks L and R at frequency $\omega$ can be casted as[25]

$$q_{L\to R}(\omega) = \frac{2}{t_{simu}\omega S}\mathrm{Im}\langle V_L(\omega)K_{LR}V_R(\omega)\rangle \quad (3)$$

where $t_{simu}$ and $S$ are the simulation time and cross section of samples. $V_L(\omega)$ and $V_R(\omega)$ denote the Fourier transformed velocity vectors at $\omega$ for the blocks L and R, respectively. $K_{LR}$ represents the force constant matrix connecting the blocks L and R. More details about this technique can be found from refs.[16,25,26] In our simulations, the heat current is averaged over 10 simulations and smoothened by a Gaussian function with a window of 0.6 THz.

The calculated SDHC for GDY and nanoribbons with a fixed length of 52 nm is illustrated in Figure 3. Note that the

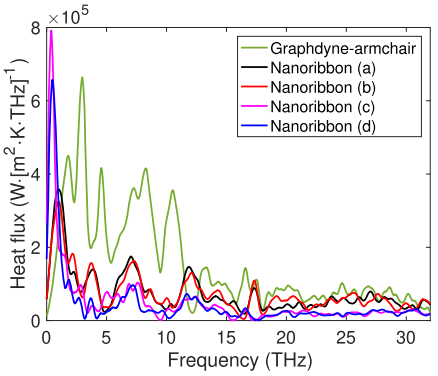


**Figure 3.** Frequency-resolved heat current of GDY and GDY nanoribbons with 52 nm in length. The spectral for GDY is along the armchair direction.

cutoff frequency of these systems is ~60 THz; to facilitate the comparisons, we only show the heat current below 30 THz as the heat current at high frequencies is small. For GDY, the SDHC is relatively large below 12 THz, indicating that the main heat carriers possess frequency below 12 THz. When downsizing into nanoribbons, the SDHC is greatly reduced in almost the entire frequency range, especially between 3 and 12 THz. That means, the main heat carriers in GDY is scattered by the nanoribbon boundaries. Interestingly, almost all the heat current peaks in nanoribbons shift to lower frequencies compared to those of GDY, which reveals the phenomenon of phonon softening in nanoribbons. From the SDHC, the heat current of nanoribbons along the armchair direction (a,b) is larger than that along the zigzag direction beyond 1.5 THz, indicating a stronger phonon scattering by zigzag edges at those frequencies. However, the phonon scattering mechanism is hardly to hinder the transport of long wavelength phonons, that is, typically the low-frequency modes. Actually, the SDHC of all nanoribbons is larger than that of GDY below 1.5 THz, which is due to the band folding effect and increased acoustic vibrational freedoms in nanoribbons: similar to nanowires, there are four acoustic branches in nanoribbons, one branch more than in GDY. Besides, the period length along the transport direction is larger than that of GDY, which means the band will be folded and flattened. Because of the two reasons, the phonon density of states of nanoribbons at low frequencies will be increased. For the nanoribbons along the zigzag direction, the band folding effect is more pronounced because of a larger period length (17.32 Å) compared to the one along the armchair direction (10 Å), which might be the reason why zigzag nanoribbons possess a larger SDHC than armchair nanoribbons below 1.5 THz. For nanoribbons along both



DOI: 10.1021/acsomega.9b00074
ACS Omega 2019, 4, 4147−4152

armchair and zigzag directions, the additional chains attached to edges only affect the SDHC below 2 THz, beyond which the heat current is almost unchanged. This phenomenon is consistent with the phonon resonant effect, which can hinder the low-frequency phonon transport while not effective for high-frequency modes[16,17] when compared to the scattering mechanism. Consequently, our edge engineering by adding side chains complements the original edge scattering, which is the reason why edge engineering can further reduce the TCs of nanoribbons. It is worth noting that although the samples with a specific length of 52 nm are used for the SDHC analysis, other lengths give similar trends.

Recently, strain engineering has become an important strategy to tune the properties of materials, such as electronic and mechanical properties.[9−11] It has been found that lattice strain can be used to both enhance[27−29] and hinder[30−34] the thermal transport in low-dimensional materials. To uncover how tensile strain affects the TC of GDY and its nanoribbons, we applied 2, 5, 8, and 12% of tensile strains on GDY along the armchair direction and on nanoribbons (a,c). The TC in each case is calculated and demonstrated in Figure 4. Note that

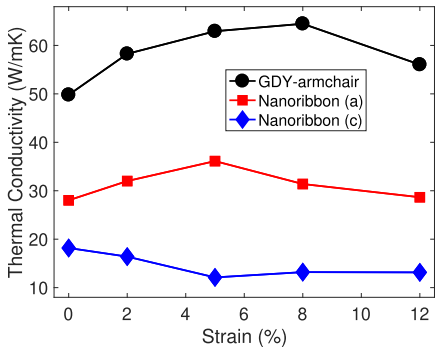


**Figure 4.** Strain effect on the TC of GDY and nanoribbons (a,c) shown in Figure 1.

when the strain is larger than 5%, the time step of simulations needs to be reduced to make sure the conservation of energy. Here, we adopted 0.2 and 0.1 fs for the strain of 8 and 12%, respectively. It is worth to note that the structures under all strains studied are stable. After more than 10 ns of simulations, all structures preserve the initial conformation with all atoms slightly deviate from their equilibrium positions. From Figure 4, it is interesting to find that the TC of zigzag nanoribbons possesses a different strain-dependent behavior compared to that of GDY and armchair nanoribbons. For GDY and armchair nanoribbons, the TC shows nonmonotonic behavior and both of them increases with the applied strain first and then decreases, resulting in a maximum TC of 64.5 and 36.1 W/m K, respectively. However, the critical strain of GDY for TC reduction is larger than that of armchair nanoribbon, whereas for the zigzag nanoribbon, the TC decreases with the applied tensile strain and reaches to a plateau after 5%. The strain-induced TC plateau has also been found in silicene.[35] Tensile strain generally has two effects on thermal transport. The first one is to increase the phonon group velocity due to the enhancement of bond stiffness.[36] For example, it has been found that the flexural mode in graphene can be linearized under tensile strain. On the other hand, strain can distort the original lattice, thus breaking the symmetry of the structure. As a result, the anharmonicity of the material will be enhanced. The enhanced phonon group velocity and anharmonicity under tensile strain, respectively, have positive and negative effects on thermal transport. In our case, with the increase of tensile strain in GDY and armchair nanoribbons, the group velocity enhancement is dominated at first and then the increased anharmonicity becomes more important, which results in a maximum TC in those structures. However, for the zigzag nanoribbon, the anharmonicity is predominated below 5%, after which with the group velocity effect on TC is comparable to that of the anharmonic effect, which might be the reason why the TC decreases monotonically first and reaches to a plateau under tensile strain.

To understand the different TC behaviors on strain for the three structures, we also calculated the frequency-resolved heat current under different strains. The results for the systems with the length of 52 nm are presented in Figure 5. In general, the SDHC is right-shifted under the stretch for all structures, which indicates that the atomic bonds become stiffer under stretch. Actually, it has been found in graphene that the flexural acoustic mode will be stiffened and linearlized under strain.[37] The SDHC shift is more obvious in GDY compared to that in nanoribbons (both armchair and zigzag). For GDY, under small strains, the variation of SDHC beyond 4 THz is small. However, the SDHC is greatly enhanced for the first two peaks (below 4 THz) until 8% of strain, after which it get reduced noticeably. A similar behavior appears in the strained armchair nanoribbons, except that the critical strain for SDHC below 4 THz changes its trend and is reduced from 8 to 5%, which is in accordance with the critical strain of TC curves. For zigzag nanoribbons, the SDHC beyond 3 THz is almost unchanged because of the strong scattering of phonons by edges; thus, the main effect of strain on zigzag nanoribbons is to change the first peak of SDHC. Different from the situation of GDYs and armchair nanoribbons, the first peak of SDHC in zigzag nanoribbons reduces first with the increase of strain and then gets enhanced slightly. This behavior also agrees with the trend of TC versus strain of zigzag nanoribbons. From the above SDHC analysis, we can see that the strain mainly affects the low-frequency phonon transport, regardless in 2D structure (GDY) or nanoribbons. The low-frequency SDHC variation governs the TC of strained structures.

## 3. CONCLUSIONS

In conclusion, we have studied the thermal transport phenomena in GDY and its nanoribbons using NEMD. The TC in GDY is isotropic while large anisotropy appears in nanoribbons with the TC of the armchair nanoribbon much larger than that of the zigzag nanoribbon. The anisotropic transport in nanoribbons arises from the different phonon boundary scattering, which hinders significantly the high-frequency phonon transport (>3 THz) as demonstrated by the SDHC. The TC of both armchair and zigzag nanoribbons can be further reduced by attaching side chains onto the nanoribbon edges, which can stop the phonon transport at low frequencies (<3 THz), thanks to the resonant mechanism. The TCs of GDY and armchair nanoribbons possess a different strain response from that of zigzag nanoribbons. The TC of GDY and armchair nanoribbons increases with tensile strain first and then reduces with the further increase of strain. However, the TCs of zigzag nanoribbons decrease with strain first and then keep almost unchanged. This difference originates from a different response of low-frequency phonon with strain. In GDY and armchair nanoribbon structures, the


DOI: 10.1021/acsomega.9b00074
ACS Omega 2019, 4, 4147−4152

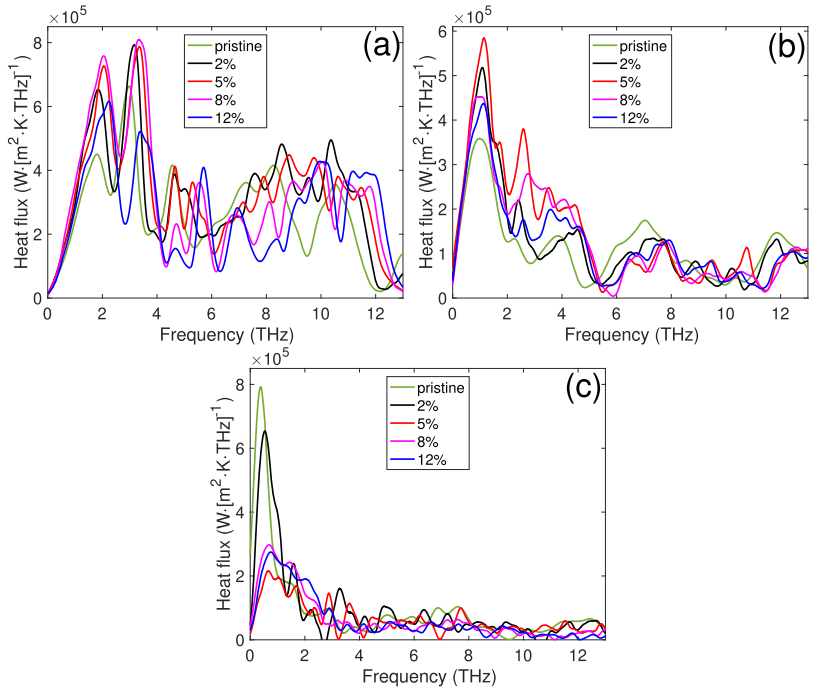


**Figure 5.** Frequency-resolved heat current for strained GDY (a) and nanoribbons along armchair (b) and zigzag (c) directions. (b,c) corresponds to the structures (a,c) in Figure 1.

SDHC below 4 THz increases first with strain and then reduces, whereas for zigzag nanoribbons, it decreases with the applied strain, which is in accordance with the strain response of TC.

## AUTHOR INFORMATION


### Corresponding Authors

*E-mail: yuzhao@suda.edu.cn (Y.Z.).
*E-mail: xiaohong_zhang@suda.edu.cn (X.Z.).

### ORCID

Yuxiang Ni: 0000-0001-8567-6998
Yu Zhao: 0000-0002-6184-2530
Xiaohong Zhang: 0000-0002-6732-2499

### Author Contributions

‖Y.W. and S.X. contribute equally.


### Notes

The authors declare no competing financial interest.

## ACKNOWLEDGMENTS

This work is support by the National Natural Science Foundation of China (grant nos. 11804242, 51772199, and 11774294) and the Jiangsu Provincial Natural Science Foundation (grant no. BK20160308). We acknowledge the financial support from the Collaborative Innovation Centre of Suzhou Nano Science & Technology, the Priority Academic Program Development of Jiangsu Higher Education Institutions (PAPD), the 111 Project, and Joint International Research Laboratory of Carbon-Based Functional Materials and Devices.

## REFERENCES

(1) Huang, C.; Li, Y.; Wang, N.; Xue, Y.; Zuo, Z.; Liu, H.; Li, Y. Progress in Research into 2D Graphdiyne-Based Materials. *Chem. Rev.* **2018**, *118*, 7744−7803.

(2) Jang, B.; Koo, J.; Park, M.; Lee, H.; Nam, J.; Kwon, Y.; Lee, H. Graphdiyne as a high-capacity lithium ion battery anode material. *Appl. Phys. Lett.* **2013**, *103*, 263904.

(3) Zhang, H.; Xia, Y.; Bu, H.; Wang, X.; Zhang, M.; Luo, Y.; Zhao, M. Graphdiyne: A promising anode material for lithium ion batteries with high capacity and rate capability. *J. Appl. Phys.* **2013**, *113*, 044309.

(4) Xiao, J.; Shi, J.; Liu, H.; Xu, Y.; Lv, S.; Luo, Y.; Li, D.; Meng, Q.; Li, Y. Efficient CH3NH3PbI3 Perovskite Solar Cells Based on Graphdiyne (GD)-Modified P3HT Hole-Transporting Material. *Adv. Energy Mater.* **2015**, *5*, 1401943.

(5) Ouyang, T.; Hu, M. Thermal transport and thermoelectric properties of beta-graphyne nanostructures. *Nanotechnology* **2014**, *25*, 245401.

(6) Jiang, P. H.; Liu, H. J.; Cheng, L.; Fan, D. D.; Zhang, J.; Wei, J.; Liang, J. H.; Shi, J. Thermoelectric properties of $\gamma$ -graphyne from first-principles calculations. *Carbon* **2017**, *113*, 108−113.

(7) Sun, L.; Jiang, P. H.; Liu, H. J.; Fan, D. D.; Liang, J. H.; Wei, J.; Cheng, L.; Zhang, J.; Shi, raphdiyneJ. Graphdiyne: A two-dimensional thermoelectric material with high figure of merit. *Carbon* **2015**, *90*, 255−259.

(8) Zhang, Y. Y.; Pei, Q. X.; Wang, C. M. A molecular dynamics investigation on thermal conductivity of graphynes. *Comput. Mater. Sci.* **2012**, *65*, 406−410.

(9) Ghadimi, A. H.; Fedorov, S. A.; Engelsen, N. J.; Bereyhi, M. J.; Schilling, R.; Wilson, D. J.; Kippenberg, T. J. Elastic strain engineering for ultralow mechanical dissipation. *Science* **2018**, *360*, 764−768.

(10) Meesala, S.; et al. Strain engineering of the silicon-vacancy center in diamond. *Phys. Rev. B: Condens. Matter Mater. Phys.* **2018**, *97*, 205444.

(11) Kripalani, D. R.; Kistanov, A. A.; Cai, Y.; Xue, M.; Zhou, K. Strain engineering of antimonene by a first-principles study: Mechanical and electronic properties. *Phys. Rev. B: Condens. Matter Mater. Phys.* **2018**, *98*, 085410.

(12) Vermeulen, P. A.; Mulder, J.; Momand, J.; Kooi, B. J. Strain engineering of van der Waals heterostructures. *Nanoscale* **2018**, *10*, 1474−1480.



DOI: 10.1021/acsomega.9b00074
*ACS Omega* 2019, 4, 4147−4152

(13) Ouyang, B.; Xiong, S.; Yang, Z.; Jing, Y.; Wang, Y. MoS2 heterostructure with tunable phase stability: strain induced interlayer covalent bond formation. *Nanoscale* **2017**, *9*, 8126−8132.
(14) Xue, X.-X.; Feng, Y.-X.; Liao, L.; Chen, Q.-J.; Wang, D.; Tang, L.-M.; Chen, K. Strain tuning of electronic properties of various dimension elemental tellurium with broken screw symmetry. *J. Phys.: Condens. Matter* **2018**, *30*, 125001.
(15) Li, Q.; Tang, L.; Zhang, C.; Wang, D.; Chen, Q.-J.; Feng, Y.-X.; Tang, L.-M.; Chen, K.-Q. Seeking the Dirac cones in the MoS2/WSe2 van der Waals heterostructure. *Appl. Phys. Lett.* **2017**, *111*, 171602.
(16) Xiong, S.; Sääskilahti, K.; Kosevich, Y. A.; Han, H.; Donadio, D.; Volz, S. Blocking Phonon Transport by Structural Resonances in Alloy-Based Nanophononic Metamaterials Leads to Ultralow Thermal Conductivity. *Phys. Rev. Lett.* **2016**, *117*, 025503.
(17) Xiong, S.; Selli, D.; Neogi, S.; Donadio, D. Native surface oxide turns alloyed silicon membranes into nanophononic metamaterials with ultralow thermal conductivity. *Phys. Rev. B: Condens. Matter Mater. Phys.* **2017**, *95*, 180301.
(18) Chen, X.-K.; Liu, J.; Xie, Z.-X.; Zhang, Y.; Deng, Y.-X.; Chen, K.-Q. A local resonance mechanism for thermal rectification in pristine/branched graphene nanoribbon junctions. *Appl. Phys. Lett.* **2018**, *113*, 121906.
(19) Liu, Y.-Y.; Zeng, Y.-J.; Jia, P.-Z.; Cao, X.-H.; Jiang, X.; Chen, K.-Q. An efficient mechanism for enhancing the thermoelectricity of nanoribbons by blocking phonon transport in 2D materials. *J. Phys.: Condens. Matter* **2018**, *30*, 275701.
(20) Zhou, W.-X.; Chen, K.-Q. Enhancement of thermoelectric performance in $\beta$-graphyne nanoribbons by suppressing phononic thermal conductance. *Carbon* **2015**, *85*, 24−27.
(21) Plimpton, S. Fast Parallel Algorithms for Short-Range Molecular Dynamics. *J. Comput. Phys.* **1995**, *117*, 1−19.
(22) Stuart, S. J.; Tutein, A. B.; Harrison, J. A. A reactive potential for hydrocarbons with intermolecular interactions. *J. Chem. Phys.* **2000**, *112*, 6472−6486.
(23) Sellan, D. P.; Landry, E. S.; Turney, J. E.; McGaughey, A. J. H.; Amon, C. H. Size effects in molecular dynamics thermal conductivity predictions. *Phys. Rev. B: Condens. Matter Mater. Phys.* **2010**, *81*, 214305.
(24) Dong, H.; Fan, Z.; Shi, L.; Harju, A.; Ala-Nissila, T. Equivalence of the equilibrium and the nonequilibrium molecular dynamics methods for thermal conductivity calculations: From bulk to nanowire silicon. *Phys. Rev. B: Condens. Matter Mater. Phys.* **2018**, *97*, 094305.
(25) Sääskilahti, K.; Oksanen, J.; Tulkki, J.; McGaughey, A. J. H.; Volz, S. Vibrational mean free paths and thermal conductivity of amorphous silicon from non-equilibrium molecular dynamics simulations. *AIP Adv.* **2016**, *6*, 121904.
(26) Sääskilahti, K.; Oksanen, J.; Tulkki, J.; Volz, S. Role of anharmonic phonon scattering in the spectrally decomposed thermal conductance at planar interfaces. *Phys. Rev. B: Condens. Matter Mater. Phys.* **2014**, *90*, 134312.
(27) Zhang, T.; Luo, T. Morphology-influenced thermal conductivity of polyethylene single chains and crystalline fibers. *J. Appl. Phys.* **2012**, *112*, 094304.
(28) Kuang, Y.; Lindsay, L.; Huang, B. Unusual Enhancement in Intrinsic Thermal Conductivity of Multilayer Graphene by Tensile Strains. *Nano Lett.* **2015**, *15*, 6121−6127.
(29) Shen, S.; Henry, A.; Tong, J.; Zheng, R.; Chen, G. Polyethylene nanofibres with very high thermal conductivities. *Nat. Nanotechnol.* **2010**, *5*, 251.
(30) Zhu, L.; Zhang, T.; Sun, Z.; Li, J.; Chen, G.; Yang, S. A. Thermal conductivity of biaxial-strained MoS2: sensitive strain dependence and size-dependent reduction rate. *Nanotechnology* **2015**, *26*, 465707.
(31) Wei, N.; Xu, L.; Wang, H.-Q.; Zheng, J.-C. Strain engineering of thermal conductivity in graphene sheets and nanoribbons: a demonstration of magic flexibility. *Nanotechnology* **2011**, *22*, 105705.
(32) Xie, H.; Ouyang, T.; Germaneau, E.; Qin, G.; Hu, M.; Bao, H. Large tunability of lattice thermal conductivity of monolayer silicene via mechanical strain. *Phys. Rev. B: Condens. Matter Mater. Phys.* **2016**, *93*, 075404.
(33) Li, X.; Maute, K.; Dunn, M. L.; Yang, R. Strain effects on the thermal conductivity of nanostructures. *Phys. Rev. B: Condens. Matter Mater. Phys.* **2010**, *81*, 245318.
(34) Parrish, K. D.; Jain, A.; Larkin, J. M.; Saidi, W. A.; McGaughey, A. J. H. Origins of thermal conductivity changes in strained crystals. *Phys. Rev. B: Condens. Matter Mater. Phys.* **2014**, *90*, 235201.
(35) Hu, M.; Zhang, X.; Poulikakos, D. Anomalous thermal response of silicene to uniaxial stretching. *Phys. Rev. B: Condens. Matter Mater. Phys.* **2013**, *87*, 195417.
(36) Shao, C.; Yu, X.; Yang, N.; Yue, Y.; Bao, H. A Review of Thermal Transport in Low-Dimensional Materials Under External Perturbation: Effect of Strain, Substrate, and Clustering. *Nanoscale Microscale Thermophys. Eng.* **2017**, *21*, 201−236.
(37) Bonini, N.; Garg, J.; Marzari, N. Acoustic Phonon Lifetimes and Thermal Transport in Free-Standing and Strained Graphene. *Nano Lett.* **2012**, *12*, 2673−2678.



DOI: 10.1021/acsomega.9b00074
*ACS Omega* 2019, 4, 4147−4152